Discover Chemistry

RESEARCH Open Access

Synthesis, and characterization of magnesium oxide nanoparticles (MgO NPs) derived from *Raphia hookeri* seeds (RHS) and evaluation of their nano-pharmacokinetic properties

Bamidele Honesty Akpeji[1,2,3*] and Vikash Singh[4]

*Correspondence:
Bamidele Honesty Akpeji
akpeji.honesty@fupre.edu.ng
[1]Department of Science Laboratory Technology, Federal University of Petroleum Resources, P.M.B 1221, Effurun, Delta State, Nigeria
[2]Centre for Sustainable Development Goals, Federal University of Petroleum Resources, P.M.B 1221, Effurun, Delta State, Nigeria
[3]Centre for Waste Management and Sustainable Resources, Federal University of Petroleum Resources, P.M.B 1221, Effurun, Delta State, Nigeria
[4]Department of Pharmaceutical Sciences, Guru Ghasidas University (A central University), Bilaspur 459009, India

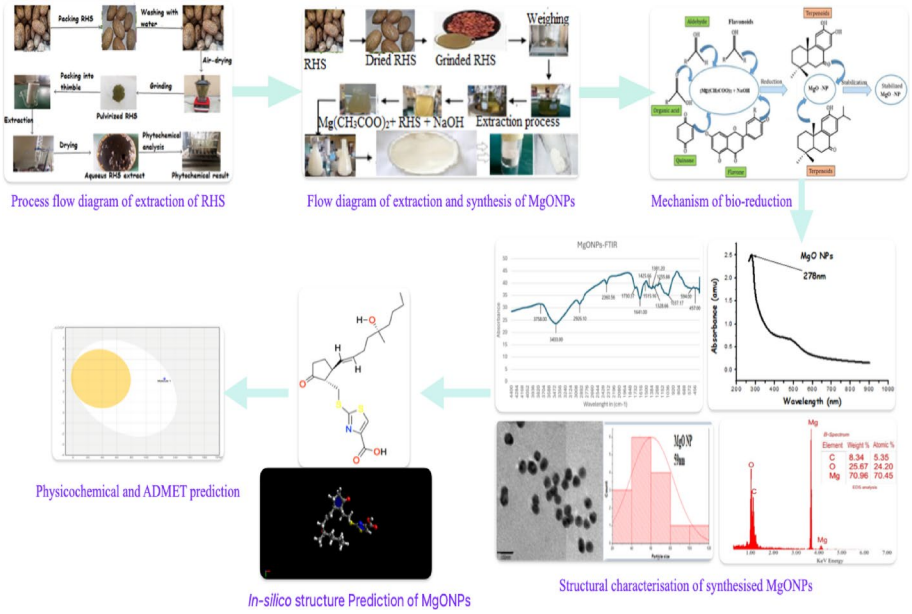
Abstract

The present study involves the development of MgO NPs from *RHS* and the evaluation of their nano-pharmacokinetic properties. The MgO NPs were synthesized via the solvothermal method using the aqueous extract of RHS. The synthesized MgO NPs were characterized using a UV-VIS spectrophotometer, a scanning electron microscope (SEM), a transmission electron microscope (TEM), powdered X-ray diffraction techniques (PXRD), an energy dispersive X-ray (EDX) spectrophotometer, and a Fourier transform infrared spectrophotometer (FTIR). The design of MgO NPs was established using ChemDraw before implementing FROG2 for energy minimization and visualizing the results through PyMOL and Avogadro. SwissADME in-silico pharmacokinetic profiling and ADMET analysis were conducted for predicting drug absorption, distribution, metabolism, excretion and toxicity profiles. phytochemical results showed that aqueous extract of RHS contained polyphenols, flavonoids, tannins, saponins, alkaloids, and reducing sugars, which enabled the biosynthesis of MgO NPs. Characterization of biosynthesized MgO NPs revealed that the uv-vis spectrophotometer showed an absorption peak at 278 nm. SEM showed that the MgO NPs are spherical and porous. TEM revealed the average particle size of MgO NPs to be 59 nm. X-ray diffraction analysis showed the crystalline state of MgO NPs, while EDX indicated the elemental constituents in MgO NPs with magnesium, oxygen and carbon as 70.96%, 25.67% and 8.34%, respectively. The FTIR result showed functional groups like the carbonyl (C=O) and hydroxyl (-OH). The MgO NPs achieved a stable conformation according to in-silico analysis, which led to pharmacokinetic evaluation. SwissADME analysis reported that MgO NPs exhibited solubility together with favorable drug-like properties based on Lipinski's Rule of Five.

Keywords Synthesis, Characterization, Nanoparticles, MgO NPs, RHS, Pharmacokinetics

© The Author(s) 2026. **Open Access** This article is licensed under a Creative Commons Attribution 4.0 International License, which permits use, sharing, adaptation, distribution and reproduction in any medium or format, as long as you give appropriate credit to the original author(s) and the source, provide a link to the Creative Commons licence, and indicate if changes were made. The images or other third party material in this article are included in the article's Creative Commons licence, unless indicated otherwise in a credit line to the material. If material is not included in the article's Creative Commons licence and your intended use is not permitted by statutory regulation or exceeds the permitted use, you will need to obtain permission directly from the copyright holder. To view a copy of this licence, visit http://creativecommons.org/licenses/by/4.0/.

Graphical abstract



1 Introduction

Nanotechnology is constantly expanding its sphere of influence in medicine, agriculture, and environmental science, which contributes to new uses using the tools of manipulating materials in the nanoscale [1, 2]. Among the numerous nanomaterials studied, metal oxides, especially MgO NPs have become the topic of interest because of the high surface area, biocompatibility, and antimicrobial properties of metal oxides [3, 4]. MgO NPs are traditionally produced by chemical reactions like precipitation, sol-gel processing or thermal decomposition. Although these are accurate and give high yields, they normally utilize toxic chemicals, and they demand a lot of energy and produce dangerous by-products. Green synthesis, on the other hand, is based on plant extracts or biological agents, and it is more environmentally friendly, economical and can also be applied in biomedical practice due to the absence of residual chemical contaminants. Therefore, green synthesis is also becoming a better alternative, especially where human contact is required, which supports the necessity of novel plant-based synthesis pathways [5]. Based on this paradigm, the seeds of *Raphia hookeri*, the plants that are prevalent in West Africa, have a biological potential to be used as a source of MgO NPs. Investigations have revealed that these seeds possess a variety of bioactive compounds with the ability to mediate nanoparticle formation, which makes them promising in the field of green nanotechnology [6, 7]. As opposed to chemical synthesis, which uses strong toxic agents, extracts of *Raphia hookeri* can be used to reduce and stabilize nanoparticles using naturally occurring phytochemicals, thus simplifying the process, making it safer and inherently biocompatible. The reason behind the selection of RHSs was that they are a phytochemical-rich, non-toxic, and abundant agro-waste in West Africa, which provides low-cost and sustainable bio-reductant [2, 8]. The RHS are not fully utilized but could be used to adapt MgO NPs nano-pharmacokinetic behaviour, unlike those of common food or medicine applications (e.g., Aloe vera, Magnolia, Hyphaene), which compete with the seeds [9]. After the synthesis, thorough characterization is needed in

order to determine nanoparticle morphology, size distribution, and crystalline structure. Such methods will be employed to give in-depth structural information, such as SEM, TEM, and pXRD [10]. These are important attributes of nanoparticles that dictate their nanoparticle performances in biomedical and environmental practices [11, 12]. To supplement the characterization of MgO NPs, the nano- bioinformatics methods will be incorporated to simulate the interactions of nanoparticles in the biological systems. Nano-bioinformatics can predict the behaviour of nanoparticles, their stability, and possible therapeutic interactions to improve the interpretability of experimental data by relying on the use of computational tools [2, 13]. Further, the literature has reported the antimicrobial properties of different metal oxide nanoparticles in which this work further buttresses, particularly on MgO NPs [14–17]. Lastly, there is the added benefit of an ecologically sustainable production based on plants, which is in line with the global initiative to reduce unhealthy waste levels and increase the use of renewable sources [18]. The use of agro-waste resources like RHSs in the work contributes to the development of green nanotechnology and adds a certain biosynthetic pathway to the production of MgO nanoparticles [10, 19]. In general, the study will aim at synthesizing, characterizing, and modelling MgO NPs extracted from RHS, and this will illustrate how they can be used in the fields of medicine, environmental control, and antimicrobial development.

2 Materials and methods

2.1 Materials

Chemicals and reagents like sodium hydroxide (NaOH), magnesium acetate dihydrate [Mg $(CH_3COO)_2$. 2 H_2O], chloroform ($CHCl_3$), aqueous ammonia [$NH_{3(aq)}$], Mayer's reagent, concentrated sulphuric acid (H_2SO_4), concentrated nitric acid (HNO_3), ferric chloride ($FeCl_3$), Fehling's solution, Buiret's solution, and Tollen's reagent are of analytical grade and obtained from Sigma Aldrich Chemicals. Distilled water was acquired from the Chemistry Laboratory, Federal University of Petroleum Resources, Delta State, Nigeria.

2.2 Method

2.2.1 Collection and extraction of RHS

RHS was acquired from the cub in the Toru Ndoro locality of Bayelsa State and was identified in the Department of Plant Biology, University of Benin. The method of extraction of the RHS was the Soxhlet extraction as described [6]. In this experiment, 150 g of powdered RHS was weighed and placed in a round-bottom flask containing a thimble connected to a condenser using water as the extracting solvent. The water in the round-bottom flask was boiled using a heating mantle, where it was first converted to a gas and then condensed back to the liquid state in the condenser. The extraction solvent has a high capacity for dissolving a host of phytochemicals from plant tissues [6]. While extracting, a condenser was maintained in a cold condition to ensure that all the bioactive compounds were separated. The extraction process was complete in four hours when the sample compartment was found colourless. The mixture was transferred to a rotary evaporator to separate the solvent from the extract at a controlled temperature of 70 °C. The aqueous extract obtained was charactetrizaed for phytochemical analysis [10, 19, 20].

2.2.2 Phytochemical and bioactive components of aqueous extract of RHS

The procedure for phytochemical screening for aqueous extract of RHS was similar to the method provided [6, 21]. Figure 1 shows a flow diagram describing the process of phytochemical analysis.

Test for Alkaloids To about 2 mL of the aqueous extract of RHS, two drops of Dragendorff's reagent were added along the sides of the test tube. There was an orange-red colour precipitate formed, and this was an indication of the presence of alkaloids.

Test for Reducing Sugars To about 2 mL of the aqueous extract in the test tube, Benedict reagent was added, and the contents were gently warmed. Red precipitate in the test tube proves the fact that the extract solution contained at least a part of reducing sugars.

Test for saponin To 2 mL of the aqueous extract in the test tube, 5 mL of distilled water was added and shaken vigorously. A compact, continuous and well-formed froth for about 2 min proves the presence of saponin.

Test for Phenolic Compounds To 2 mL of the aqueous extract, a few drops of 10% ferric chloride solution were added. Green-blue colouration, which is an indicator of phenolic compounds, comes into view.

Test for carbohydrates Accurately, 5 mL of Fehling's solution was combined with 2 mL of the aqueous extract and then heated in a water bath. The formation of yellow precipitate was also seen, which confirmed the presence of carbohydrate.

Test for tannins To about 2 mL of the aqueous extract, 5% ferric chloride solution was added; the formation of a dark green precipitate proved that the plant contained tannins.

Test for Flavonoids To 2 mL of aqueous extract, add a small amount of water. Several drops of lead acetate solution were introduced, and a light yellow precipitate that signals

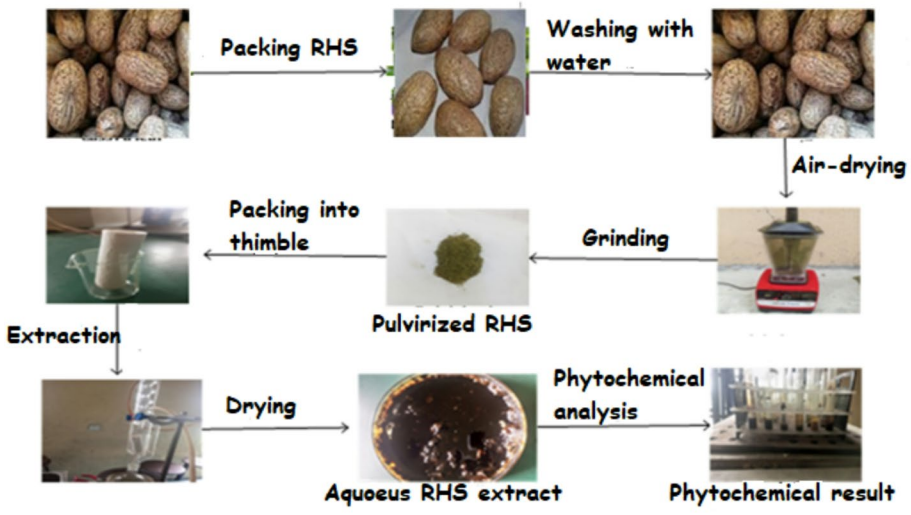


Fig. 1 Process flow diagram for the extraction and phytochemical analysis of *RHS*

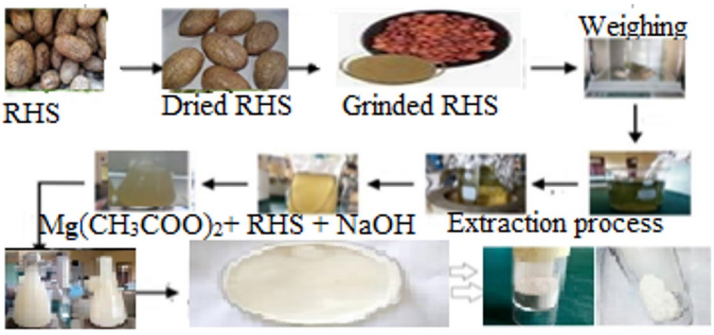


Fig. 2 Process diagram for the preparation of the *RHS* extract and synthesis of MgO NPs

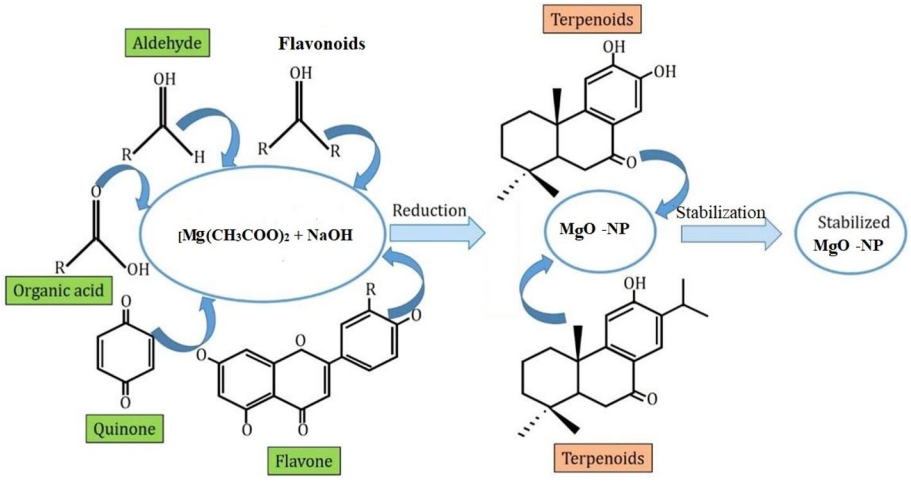


Fig. 3 Mechanism of bio-reduction of magnesium acetate into MgO-NPs using *RHS*

a flavonoid compound was formed. A yellow precipitate was observed, which indicated the presence of carbohydrate.

2.2.3 Bio-synthesis of MgO NPs from RHS

The synthesis procedures presented herein are solvothermal methods, which are nearly identical to those of [14, 22] and only require minor modifications. RHS employed in this synthesis was taken from its culture and washed with distilled water. It was air-dried for seven days and was crushed into powder using a local machine grinder. 4 g of the RHS powder was weighed and transferred into a clean conical flask, and 400 mL of distilled water was added. The content was heated on the heating mantle for 2 h and then filtered. A 1:20 mixture of the RHS solution extract was added to 400 mL of 0.02 M magnesium acetate solution in the presence of 20 mL of 1 M NaOH solution. The resulting liquid was then mixed by continuously stirring at 70 °C for approximately 3 h using a stirrer magnet. The cooler change of the solution from light brown to white during the reaction and the formation of magnesium hydroxide, $Mg(OH)_2$, precipitate, were observed. After centrifuging the precipitate, it was then washed with distilled water and centrifuged again at 5000 rpm. The white residue obtained was dried at 70 °C in an LD-201-E drying oven manufactured by Vision Scientific [23–25]. A UV-Visible spectrophotometer was used to monitor the formation of MgO NPs during the period of synthesis. The entire process of synthesis is summarized in Eq. 1 and Figs. 2, 3, respectively:

$$[Mg(CH_3COO)_2.2H_2O] + (Phyto - enzymes from R.H.S) \\ +1MNaOH \rightarrow Mg(OH)_2 + dryingtoremoveH_2O \rightarrow MgO - NP \quad (1)$$

2.2.4 Instrumental characterization of the MgO NPs

To guarantee the product's quality, purity, and certainty after it has been synthesized, it is crucial to ascertain several fundamental characteristics of the product. A UV-visible spectrophotometer from Perkin Elmer Lambda 40 was used to understand the formation of the MgO nanoparticles. The reaction of synthesized MgO NPs, along with functional groups present on its surface, was characterized using a Model Nicolet iS10 FT-IR Spectrometer. The JOEL JSM-IT71OHR-BECTHAI of SEM was used for the morphology of the biosynthesized MgO NPs. The elemental composition was determined using the EDX with model number EDX-8100. The size and shape of the produced MgO NPs were characterized using JEM-ARM200F-G-TEM, and the crystallinity was analyzed with Bruker AXS D8 Advance diffractometer (Cu Kα = 1.5406, voltage 40 KV and current 40 mA) analytical machine.

2.2.5 In-silico analysis of the MgO NPs

The analysis was performed using the in-silico method to predict the possible toxicity and chemical frameworks for the greenly nano-fabricated MgO. Other parameters for the process of absorption and their receptor acceptance were also analyzed by the computational method [26].

2.2.6 Structure formation of biosynthesized MgO NPs

The biosynthesized nanoparticle of MgO NPs were drawn using ChemDraw software version 25.0. The structure of Magnesium acetate dehydrate was drawn and pivoted into magnesium oxide (MgO). The presence of a carbonyl functional group acts as the bridge between two Mg atoms. The structure was exported as a Mol2 SDF file for further analysis. The structure of the synthesized Magnesium oxide nanoparticles is shown in Fig. 4 [2].

2.2.7 Optimization and characterization of chemical structure

To optimize the chemical structure by the concept of Low-energy molecules, preferably accepted for the best possible hypothesis to analyze the structural energy level and to optimize the structure. The FROG2 (Free Online Server) for the structure Fig. 5 (https://bioserv.rpbs.univ-paris-diderot.fr/services/Frog2/) method is used to perform the op

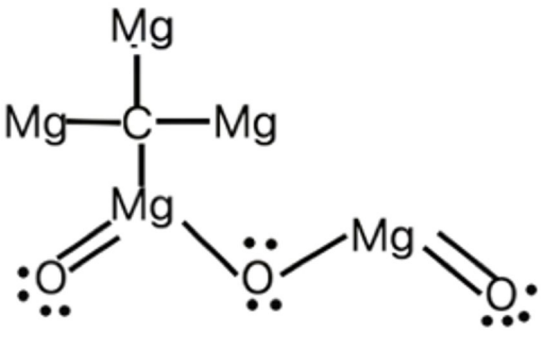


Fig. 4 Chemical structure of synthesized MgO NPs by ChemDraw

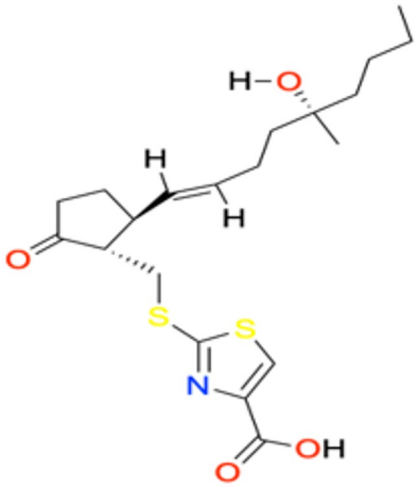


Fig. 5 Structure analysis molecule in MgO NPs

timization of the structure of the lead compound. This online server is powered by the RPBS Web portal to determine bioinformatics and drug design as tools. Here, the structure is fetched as input with the Mol file and output file as the PDB for further analysis by Pymol. The Emax was set to 50, the MC step was fixed to 100, and the energy window value was also set to 100. The verified data was exported as PDB from the FROG server and exclusively enhanced structural geometry [2].

2.2.8 Absorption prediction and drug-likeness of MgO NPs

Pharmacokinetic parameters are essential for the drug to act effectively for use because of the direct involvement of the drug molecule with the systemic circulation, starting from the absorption, distribution, metabolism, excretion, and toxicity as well. These parameters are required to make MgO NPs considerable for drug development. The effective drug candidate should process the required parameters for the ADMET, which further provides suitable information about the synthesized MgO NPs as a suitable drug material for systemic application. The analysis of greenly synthesized MgO NPs was performed via SwissADME (http://www.swissadme.ch), which is a free online server to predict the overall pharmacokinetic and Lipinski parameters, as well as provide us with the targeted information for drug-likeness properties. Therefore, the SMILE code was provided to the SwissADME, and the reports were further analyzed. ADMET were the primary characteristics of the drug to be effective and act as good therapeutic targets [2].

3 Results and discussion

3.1 Phytochemical and bioactive components of aqueous extract of *RHS*

The phytochemicals identified in the phytochemical experiment of the aqueous extract of *Raphia*.

Hookeri seed extract is tabulated below in Table 1.

The phytochemical screening of RHSs in Table 1 indicated that the sample contained saponins, alkaloids, tannins, phenolic compounds, carbohydrates, flavonoids and reducing sugars. In this work, it is believed that the biomolecule has played the role of the reducing and stabilizing/capping agents in the green synthesis of MgO NPs. The intricate combination of phytochemicals has been able to offer the required electron-donating

Table 1 Phytochemical analysis of aqueous extract *RHS*

Test performed	Results
Appearance	Liquid
Color Description	brown
Saponin	+
Alkaloids	+
Reducing Sugar	+
Anthraquinones	-
Phenolic compounds	+
Carbohydrates	+
Tannins	+
Flavonoids	+
Terpenoids	+

Keys; (+) Present, (-) Not present

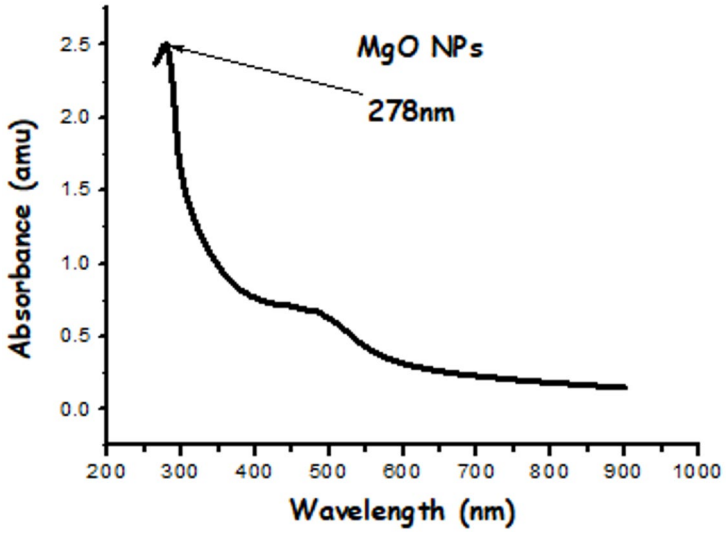


Fig. 6 UV-VIS Spectrophotometer of MgO NPs

capacity and functional groups for MgO NPs growth and nucleation, which in turn supports an eco-friendly and plant-based synthetic pathway [6, 27]. This is consistent with the idea of the use of plant-based extracts as substitutes for synthetic chemical reagents in nanomaterial preparation. Moreover, the phytochemical profile that has been determined during the present study is comparable with previous findings on RHS extracts, which also reported the presence of a rich phytochemical composition of secondary metabolites and other bioactive compounds [6]. Capping MgO NPs with these phytochemicals can affect important factors in nano pharmacokinetics, including the dispersion stability, the surface charge and their interaction with biological membranes [28].

3.2 Instrumental characterization of the biosynthesized MgO NPs

3.2.1 UV-VIS spectrophotometry

The first instrumental technique adopted to track the growth of nanoparticle formation is mostly the UV-Visible (UV-Vis) spectroscopy presented in Fig. 6. This technique is especially useful because it supplies crucial data on the manner in which nanoparticles are formed and their physical properties during the process of synthesis. UV-Vis spectroscopy explains the changes in absorbance that are linked with the formation of

nanoparticles, and to gain information on the size, shape, and electronic characteristics of the nanoparticles. In this present study, MgO NPs had their highest absorption at 278 nm. This finding closely resonates with prior research, which has also noted 260 nm and 267 nm as the highest absorbance in the synthesis of MgO NPs using different plant materials. This continuity of such results affirms the validity of UV-Vis spectroscopy in tracking nanoparticle synthesis. The natural extract obtained from RHS enabled the reduction process of magnesium acetate to magnesium oxide, which is evidence to call it a bio-reductant [29].

3.2.2 SEM

The image in Fig. 7 shows an SEM micrograph of biosynthesized MgO NPs. The SEM micrograph displays a spherical morphology with compactly arranged porous structures. The observed characteristics hold great importance concerning both environmental and catalytic applications and pharmaceutical applications when nanoparticles serve as drug delivery in nano-drug delivery systems [30]. Also, the porosity detected through SEM images holds significant importance for pharmacokinetic analysis. The therapeutic agent loading capability of porous nanoparticles depends directly on their expanded surface area because of their adsorption qualities toward drugs of all sizes [31, 32]. These characteristics strengthen the medication delivery effectively by permitting reduced amounts of nanoparticles to distribute therapeutic quantities that lead to decreased concerns regarding nanotoxicity. Controlled drug delivery depends heavily on the porous surface structure because it allows drugs to release gradually. The nanoparticle matrix conducts an extended drug release through dissolution combined with diffusion, which enables sustained plasma therapeutic levels for extended durations without requiring frequent dosing [33]. The surface porosity features within Phyto enzyme-derived active

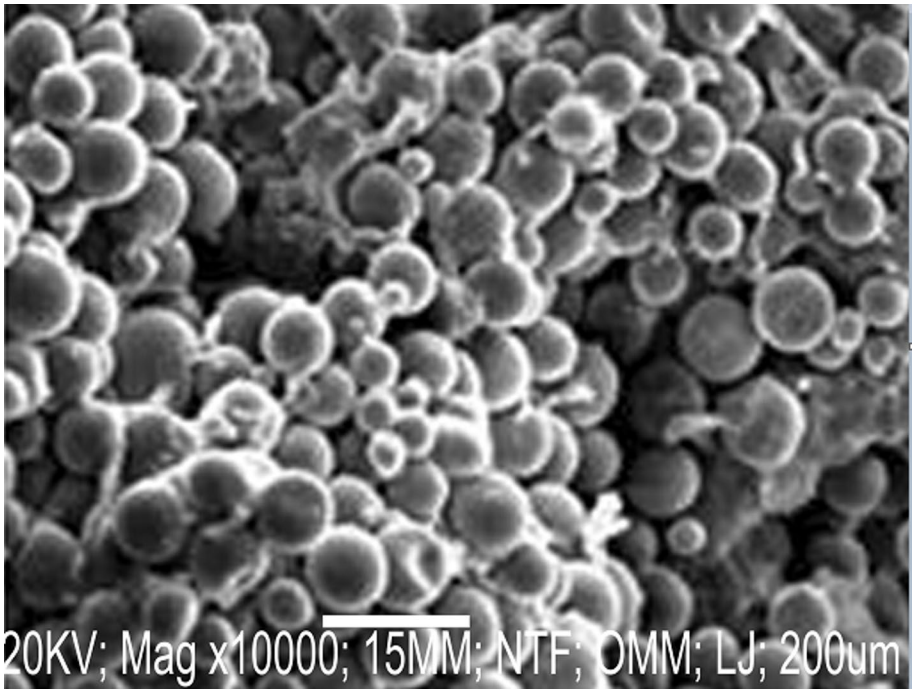


Fig. 7 SEM image of MgO NPs

sites represent a potential benefit that enables targeted delivery and site-specific binding properties [31, 34].

3.2.3 TEM

The TEM was used to determine the average particle size of the biosynthesized MgO NPs, which is shown in Fig. 8 using a TEM with model number JEOL 2100. The processing and analysis of TEM image-derived size distribution data depended on the software usage of ImageJ with version 1.54r and OriginLab with version 9.65, which amounted to a size of 59 nm along with a histogram for accurate statistical validation. The image shows that the particles were separated without agglomeration, which explains a good synthetic condition. The confirmation of this detail stands essential for pharmacokinetic research within biological systems after absorption, distribution and metabolism [5, 35]. The research provides benefits extending from pharmacokinetic studies to pharmacodynamic investigations because size and surface properties direct cellular interactions and intracellular movement.

3.2.4 PXRD

Figure 9 illustrates the PXRD pattern of the synthesized MgO NPs with sharp characteristic peaks reflecting a crystalline cubic structure of the nanoparticles. Generally, PXRD is employed to identify crystalline and non-crystalline states of materials through diffraction peaks. The state of crystallinity of the biosynthesized nanoparticles can be determined through analyzing the characteristics of PXRD peaks, such as the sharpness of the peaks, the number of peaks, the intensities, positions, and the spacing of the peaks. Ordinary materials show a broad, vague and smooth peak with several peaks and high intensity values, which suggests a more crystalline nature. Thus, while crystalline samples may generate sharp, high-intensity peaks, those samples that show low crystallinity may only reveal broad and diffuse peaks. In Fig. 8, diffraction peaks for MgO NPs are observed at 2θ = 16.4, 22.0, 42.5, and 56.2, attributed to (111), (200), (220), (311), and (222), respectively, which reflect crystallinity. The diffraction position corresponds nicely with the file with Joint Committee on Powder Diffraction Standards (JCPDS) card number 44–0141 [14, 36].

3.2.5 EDX

The EDX spectrum for biosynthesized MgO NPs is shown in Fig. 10. EDX is one of the most used techniques for determining the elemental profile of biosynthesized MgO

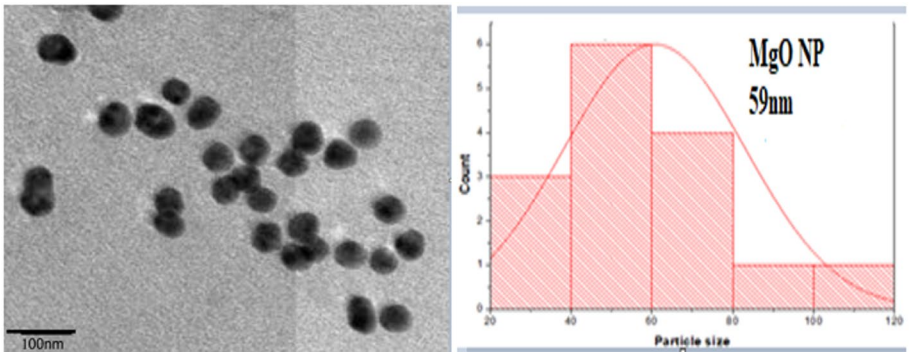


Fig. 8 TEM morphology and particle diameter of MgO NPs

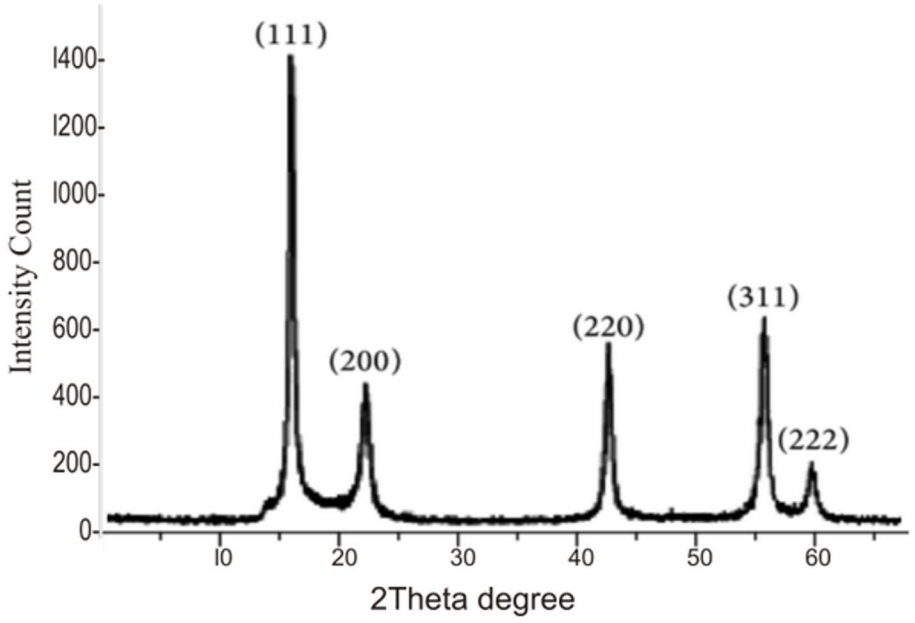


Fig. 9 PXRD spectrum of MgO NPs

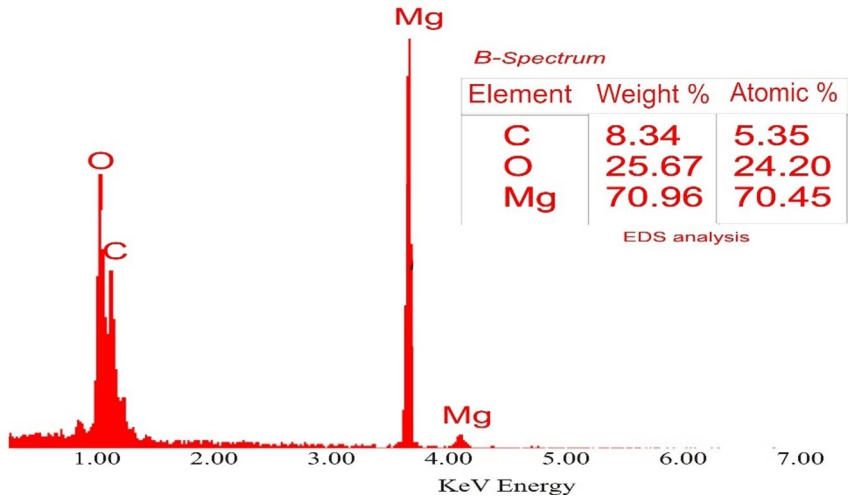


Fig. 10 EDX spectrum of MgO NPs

NPs. In the EDX spectrum, magnesium, oxygen and carbon were identified, constituting 70.96% with the energy level standing at 3.85 keV; oxygen, 25.67% with the energy value of 1.170 keV; and carbon, 8.34% at the energy level of 1.370 keV, respectively. The oxidation state of magnesium in the analysis is represented by oxygen and may be in the form of an oxide like MgO. This result is also important as it shows successful completion of the synthesis of MgO NPs. Furthermore, we expect the identification of carbon within the nanoparticles to be due to the application of the *RHS* extract during the bioformation process [37].

3.2.6 FTIR

Figure 11 gives the FTIR spectrum of the biosynthesized MgO NPs. The FTIR gives information about the functional properties present at the surface of the MgO NPs. The

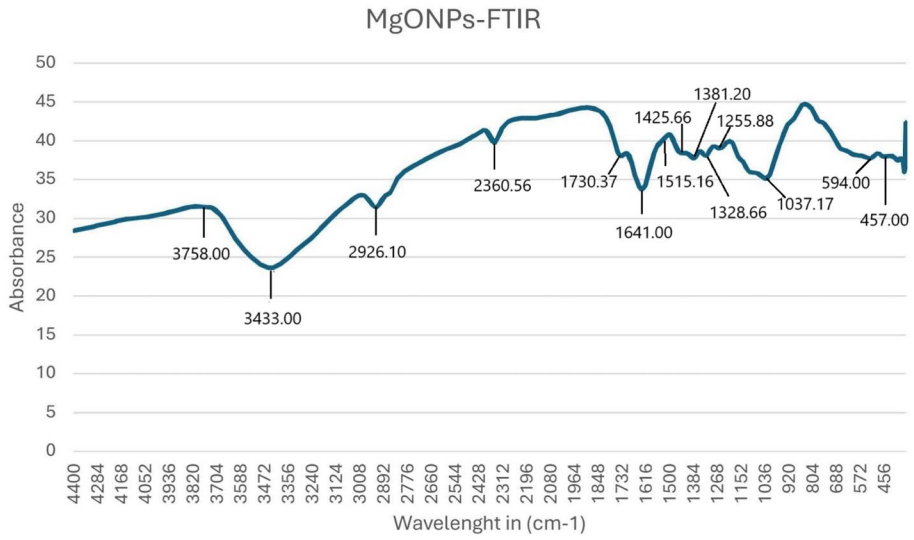


Fig. 11 FTIR spectrum of synthesized MgO NPs

presence of different band peaks at the left side of the spectrum depicts the presence of an O-H stretch band with a broad and deep peak at 3433.00 cm^{-1} [37] and the presence of aliphatic long-chain linear at 2926.10 cm^{-1} followed by 1037.17 cm^{-1}, 1255.88 cm^{-1}, 1328.66 cm^{-1}, 1381.20 cm^{-1}, 1425.66 cm^{-1} in the fingerprint region which is reportedly allocated in the structure of the compound. On the other hand, in the center of the spectrum, the peak shows the presence C-C stretch band peak at 2360.56 cm^{-1}. At the right side, the presence of C = C carbonyl is confirmed at peak 1730.37 cm^{-1}, and simple carbonyls like ketone and aldehyde are also confirmed [38, 39]. Thereafter, the aromatic ring of the C-H band stretch is also confirmed at 1515.16 $cm^{-1,}$ which confirms the ring system in the compound. In the fingerprint region, several functional groups are shown via the different stretch bands and peaks. Starting from the gem-dimethyl > C-H presents at 1381.20 $cm^{-1,}$ and the peak at 1037.17 cm^{-1} shows the cyclohexane ring vibrations [40]. Therefore, the C-N stretch band is also confirmed at peak 1328.66 $cm^{-1,}$ reporting the presence of aromatic tertiary amine in the conjugated ring system [41–46]. The FTIR peak also reports for the C-S band stretch peak at 594.00 $cm^{-1,}$ which also results in the presence of disulfide in the compound based on these band stretches and the suitable compound is plated and confirmed by other various servers like PubChem and FROG2 and all the peaks were also shown in Fig. 11.

3.3 In-silico analysis of the MgO NPs

A joint approach of ChemDraw and FTIR spectroscopy served as the first method for determining the structural characterization of biosynthesized MgO NPs. Chemdraw software enabled users to create visual chemical structures along with models which presented 2D depictions of MgO NPs. The surface functional groups of nanoparticles become identifiable through FTIR spectroscopy, ensuring both successful biosynthesis and surface modification. The research showed the existence of a carbonyl functional group that functions as a link between two magnesium atoms located at the terminal positions. The carbonyl functional group stems from phytochemical components in the plant extract during synthesis, indicating that extract molecules stabilize and cap the nanoparticles. The determined structure received storage in Molfile Version 2 (MOL2)

and Structure Data File (SDF) file formats. These standardized molecular formats serve the needs of drug design computing because they maintain essential molecular data about atomic relationships and spatial placements. Structured data must retain its original form for successful transfer between software platforms since this enables in silico analysis. The molecular files underwent an import process into Avogadro, where scientists evaluated both spatial arrangements and geometric characteristics of atomic arrangements for the nanoparticles. The 3D figure in Fig. 12 demonstrates particle conformation analysis to reveal important insight about molecular stability and potential surface interactions that happen in biological environments.

One main purpose of the conducted in silico analysis dealt with optimizing the MgO NPs' molecular geometry. The molecules in computational chemistry naturally adopt minimal internal energy conformations since these states function as their most thermodynamically stable forms. Minimization of biosynthesized MgO NPs through energy minimization methods produced the most thermodynamically favorable conformation because this feature directly affects drug-like properties, along with the biological stability of nanoparticles. When positioned in biological systems, molecules at their lowest energy stage demonstrate better stability factors while maintaining their fundamental dimensions and exterior characteristics. The stability of nanoparticles throughout their systemic circulation depends heavily on this fundamental step because unstable NPs might aggregate with each other and degrade before reaching their target sites. The optimized molecular structure was transferred to the Remote Procedure Batch System (RPBS) web server because this server operates as a dedicated platform for molecular modelling and docking preparation. The system, powered by the Remote Procedure Batch System, converted the molecular file into Protein Data Bank (PDB) format, which serves as a universal standard for molecular docking operations as well as ligand-receptor interaction evaluation and pharmacokinetic simulation processes. The Protein Data Bank file maintains the molecular shape in addition to storing atomic coordinates alongside connectivity information and energy characteristics. The conversion served an essential purpose to enable subsequent computational assessments such as binding affinity prediction and molecular docking with biological receptors, along with in-silico toxicity profiling.

The in-silico analysis represents a fundamental capability for designing nanoparticles rationally. The system evaluated MgO NPs as drug carriers by beginning with

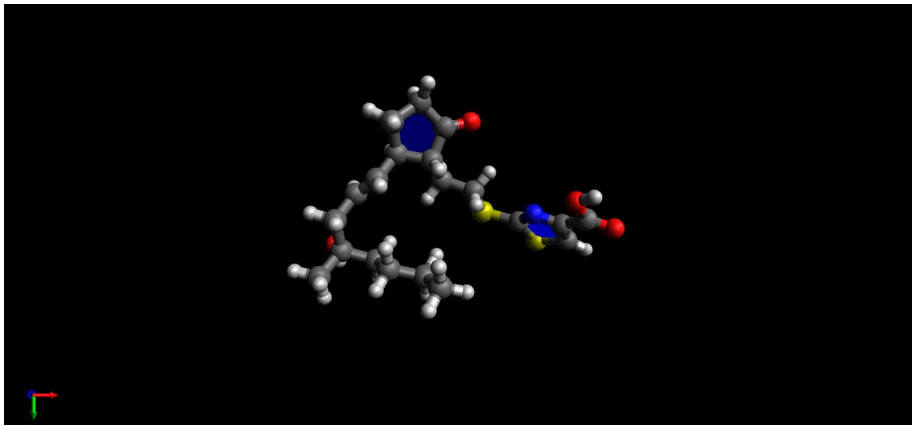


Fig. 12 Structural visualization of MgO NPs by Avogadro

experimental FTIR characterization and followed by structural modelling, then geometry optimization, and docking preparation. These integrated workflows, which use combined computational modelling and wet laboratory synthesis approaches, play an essential role in advancing nanomedicine through the development phase. The simulated drug-loading performance, together with release kinetics and biodistribution and surface property analysis of accurate nanoparticle models, establishes the most applicable nanoparticle conformations for in vitro and in vivo experimentation. The sequential in-silico methodology functions to connect synthesis and pharmacokinetic modelling of MgO NPs by revealing substantial information about their biological response. Trusted data becomes crucial during nanoparticle design because their breakable characteristics affect how the nanoparticles function inside the human body (ADME). Moreover, the biosynthesized MgO NPs acquire computer-based validation for pharmaceutical applicability through their joint application of ChemDraw with FTIR spectrometry and PyMOL visualization and their energy-minimized structure and PDB conversion phase, which results in robust candidates for pharmacokinetic and pharmacodynamic modelling studies.

3.4 Drug-likeness and absorption state prediction of MgO NPs

The greenly synthesized MgO NPs were analyzed by the SwissADME server, and the absorption parameters were analyzed by the boiled-egg model, which exhibits good HIA (Human intestinal properties). Figure 13 exhibits the clear result that molecule 1, as the lead molecule, is readily absorbed from the Gastrointestinal tract. However, it can't be able to cross the BBB (Blood Brain Barrier), which dictates that this lead molecule has no therapeutic value in the brain. On the other hand, the bioavailability results in a good score, i.e., 0.56, which depicts good absorption in the intestinal region. The compound molecular formula was $C_{20}H_{29}NO_4S_2$ with a molecular weight of 411.58 g/mol and contains 27 heavy atoms and none of the heavy aromatic atoms. It also has a C (SP^3) fraction, which is 0.65 with 10 rotatable bonds, which confirms that the compound

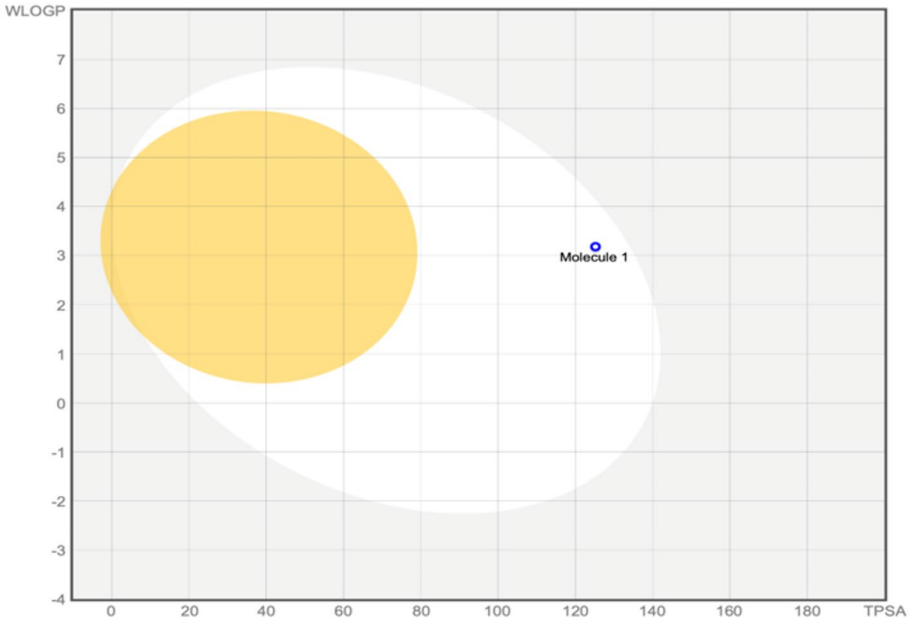


Fig. 13 Prediction of absorption by the Egg-albumin method by SwissADME

has a different conformational isomer. Therefore, it has five H-bond acceptors and two H-bond donors are also reported. The compound confirms the molar refractivity of 119.13, and the TPSA (Topological Surface Area) is 125.20 A2 and shows the Synthetic accessibility of 5.59 as shown in Table 1. This compound also indicates high water solubility with a good score in solubility, which indicates that the compound is soluble in the GI medium, which is aqueous. It also shows poor skin permeability with a score of Log K_p is −6.60 cm/s, which dictates that the compound is not suitable for tropical formulation. The compound is stuck to Lipinski's Rule of Five with zero violations. Although the lead-likeness exhibits the 2 violations due to Molecular weight > 350, and due to > 7 rotors. Therefore, it confirms that the compound is following all the suitable parameters of pharmacokinetics as the drug lead-likeness, and based on these parameters, the greenly synthesized MgO NPs exhibit potential targets for therapeutic agents (Table 2).

3.5 ADMET profile of MgONPs

The HIA demonstrates high intestinal absorption at 0.97. ADMET profiling of this candidate molecule shows a tough pharmacokinetic profile and serious safety concerns. It is likely to be well absorbed, but a very low Caco-2 of −6.296 and MDCK of −4.688, with a probability of 93.3% for low oral bioavailability (F_{20}%), suggests that poor passive diffusion may limit systemic exposure.

The molecule was likely to have a confined distribution within the vascular compartment and limited tissue distribution, including minimal blood-brain barrier penetration, along with a high plasma protein binding of 98.186% and low fraction unbound (Fu = 1.132%) in the systemic circulation with a VDss = − 1.0 L/kg. This chemical has a high potential for drug-drug interactions due to the strong inhibition of OATP1B1/1B3 transporters and as a definitive substrate for the CYP2C9 enzyme, apart from being relatively clean metabolically about the interactions with CYP3A4 and CYP1A2. Most importantly, the toxicological evaluation reveals significant risks: the high probability of genotoxicity for the molecule is 0.969, and there are four structural alerts for carcinogenicity; severe localized toxicity also exists, such as respiratory irritation and eye corrosion, while the risks of cardiotoxicity and acute rat oral toxicity are low. Therefore, even if the low clearance and metabolic stability were advantageous, the poor permeability of the scaffold and the high mutagenic/carcinogenic hazards suggest that this series may not be suitable for further clinical development, or at least the structure needs further optimisation.

Table 2 Physicochemical parameters of biosynthesised MgO NPs

Physiochemical	Parameters
Molecular Formula	$C_{20}H_{29}NO_4S_2$
Molecular Weight	411.58 g/mol
No of Heavy atoms	27
No of aromatic heavy atoms	0
Fraction Csp^3	0.56
No of Rotatable bonds	10
No of H-bond acceptor	5
No of H-bond donor	2
Molar Refractivity	119.13
TPSA	125.20 A^{o2}
Log Pk (Skin)	−6.60 cm/s
Synthetic accessibility	5.59

Table 3 ADMET profiling of MgO NPs

Property	Value	Interpretation
Absorption		
Caco-2 Permeability	−6.296	Low permeability (Optimal: > −5.15)
MDCK Permeability	−4.688	Low permeability (< 2 × 10 − 62\times$10^{-6}$,2×10^{-6} cm/s)
Pgp-inhibitor	0.001	Very low probability of being an inhibitor
Pgp-substrate	0.0	High probability of being a non-substrate
HIA	0.97	High probability (97%) of Human Intestinal Absorption
F_{20}% Bioavailability	0.933	93.3% probability that bioavailability is < 20%
30% Bioavailability	0.993	99.3% probability that bioavailability is < 30%
Distribution		
PPB (Plasma Protein Binding)	98.186%	High binding (Optimal: < 90%); may lower therapeutic index
VDss (Vol. of Distribution)	−1.0	Outside optimal range (0.04–20 L/kg)
BBB Penetration	0.0	High probability of being BBB negative (no penetration)
Fu (Fraction unbound)	1.132%	Low fraction unbound (< 5%)
OATP1B1/OATP1B3 Inhibitor	0.984/0.999	Very high probability of being an inhibitor
Metabolism		
CYP1A2 Inhibitor/Substrate	0.0/0.0	Non-inhibitor and non-substrate
CYP2C9 Substrate	1.0	100% probability of being a CYP2C9 substrate
CYP3A4 Inhibitor/Substrate	0.0/0.0	Non-inhibitor and non-substrate
HLM (Liver Microsomal Stability)	0.0	Predicted to be stable (> 30 min)
Excretion		
CL_{plasma} (Clearance)	0.228	Low clearance (< 5 ml/min/kg)
$T_1/_2$ (Half-life)	1.175	Short half-life (between 1 and 4 h)
Toxicity		
hERG Blockers	0.009	Very low probability of cardiotoxicity
AMES Mutagenicity	0.121	Low probability of mutagenicity
Rat Oral Acute Toxicity	0.0	Low toxicity (> 500 mg/kg)
Eye Corrosion/Irritation	0.993/0.957	High probability of being corrosive and an irritant
Respiratory Toxicity	0.989	High probability of being a respiratory toxicant
Genotoxicity	0.969	High probability of genotoxicity
Genotoxic Carcinogenicity	4 alerts	Multiple structural alerts for carcinogenicity

4 Conclusion

The study adequately shows the biosynthesis of MgO NPs from RHS, along with elaborating its uses in nanomedicine and as environmental remediation. The MgO NPs were successfully synthesized and characterized for UV-Vis Spectrophotometer, SEM, TEM, FTIR, EDX and PXRD to explain the optical property, morphology, size, functional moieties, elemental constituents and crystallography state. Phytochemical analysis of the aqueous RHS extract showed the presence of bioactive components like saponin, tannins, flavonoids, reducing sugars, alkaloids, phenolics and carbohydrates, which contributed to the reduction of the magnesium acetate precursor to MgO NPs. In addition, the molecular pharmacokinetic studies in ADMET analysis indicated that the MgO NPs are prospective for drug design and application, especially against drug-resistant strains. Although the work lacks in vivo pharmacological validation. The results indicated the crucial role of plant-derived materials in the formation of nanoparticles and opened the possibility of further investigation into therapies involving nanoparticles alongside safety concerns. In all, this work will help in developing better practices towards nanotechnological approaches that are sustainable and create other opportunities for more progressive treatment solutions (Table 3).

Abbreviations

RHS *Raphia hookeri* seed

MgO	Magnesium oxide
NPs	Nanoparticles
MgO NPs	Magnesium oxide nanoparticles
UV-VIS	Ultraviolet-Visible spectroscopy/spectrophotometry
SEM	Scanning electron microscope
TEM	Transmission electron microscope
pXRD	Powder X-ray diffraction
EDX	Energy-dispersive X-ray spectroscopy
FT-IR	Fourier Transform Infrared spectroscopy/spectrophotometer
ChemDraw	Chemical structure drawing software
FROG2	Free Online Server (structure optimization)
RPBS	Remote Procedure Batch System (web server)
PyMOL	Molecular visualization software
Avogadro	Molecular editor/visualization software
PDB	Protein Data Bank (file format)
MOL2	Molfile Version 2 (MOL2 file format)
SDF	Structure data file
SwissADME	SwissADME web tool (in-silico ADME profiling)
ADMET	Absorption, distribution, metabolism, excretion and toxicity
ADME	Absorption, distribution, metabolism and excretion
HIA	Human intestinal properties
BBB	Blood-brain barrier
TPSA	Topological polar surface area
SMILE (as written)	SMILES string (Simplified Molecular Input Line Entry System)

Acknowledgements
The authors wish to acknowledge Tertiary Education Trust Fund (TETfund) for sponsoring this research and to the Federal University of Petroleum Resources (FUPRE), Nigeria, for using their facilities. The mentorship in the field of nanotechnology from Professor E.E. Elemike in FUPRE is greatly acknowledged by the authors.

Author contributions
B.H Conceptualizes the research idea and did the experimental work and the entire write up. V. Did the computational aspect of the work and reviewed the work.

Data availability
All data generated or analyzed during this study are included in this published article and have been represented as graphs or spectra, but they are available on request from the corresponding author.

Declarations

Ethics approval and consent to participate
This study did not involve human participants, human biological samples, or experimental animals. The research focused on plant material (*Raphia hookeri* seed), nanomaterial synthesis, physicochemical characterization, and in-silico computational analysis. Therefore, ethical approval from an institutional review board or ethics committee was not required.

Consent for publication
Not applicable.

Competing interests
The authors declare no competing interests.

Received: 10 July 2025 / Accepted: 13 March 2026
Published online: 18 March 2026

References

1. Sellappan LK, Manoharan S. Fabrication of bioinspired keratin/sodium alginate based biopolymeric mat loaded with herbal drug and green synthesized zinc oxide nanoparticles as a dual drug antimicrobial wound dressing. Int J Biol Macromol. 2024;259:129162. https://doi.org/10.1016/j.ijbiomac.2023.129162.
2. Shabbir MA, Naveed M, Rehman S, Ain N, Aziz T, Alharbi M, et al. Synthesis of iron oxide nanoparticles from *Madhuca indica* plant extract and assessment of their cytotoxic, antioxidant, anti-inflammatory, and anti-diabetic properties via different nanoinformatics approaches. ACS Omega. 2023;8(37):33358–66. https://doi.org/10.1021/acsomega.3c02744.
3. Hemmami H, Amor BI, Zeghoud S, Laouini SE, Nleonu E, Pohl P. A Systematic Review of Synthesis MgO Nanoparticles and Their Applications. Turk Chem Soc. 2024. https://doi.org/10.18596/jotcsa.1247385.
4. Gayathri T, Venkata Ramana M, Rama Rao N. Formulation and evaluation of self nano emulsifying drug delivery system of Raloxifene hydrochloride. J Drug Deliv Ther. 2021;11(4):16–9. https://doi.org/10.22270/jddt.v11i4.4857.
5. Gayathri T, Logesh Kumar S, Sangavi S, Yudhika M, Swathy M. Green synthesis of copper oxide nanoparticles using *Carica papaya* and their antimicrobial activity. Mater Today Proc. 2023. https://doi.org/10.1016/j.matpr.2023.11.136.
6. Akpeji BH, Lari B, Igbuku UA, Tesi GO, Elemike EE, Akusu PO. Synthesis and characterization of MnO2 nanoparticles mediated by *Raphia hookeri* seed. J Nigerian Soc Phys Sci. 2024. https://doi.org/10.46481/jnsps.2024.2203.

7. Gharagozlou M, Nadafan M, Sadjadi S. The effect of $CoFe_2O_4$ and $CoFe_2O4$/SiO2 nanoparticles on structural, linear and nonlinear optical properties of MOF-199. Inorg Chem Commun. 2024;167:112741. https://doi.org/10.1016/j.inoche.2024.112741.
8. Mehra V, Kumar S, Tamang AM, Chandraker SK. Green synthesis of gold nanoparticles (AuNPs) by using plant extract and their biological application: a review. BioNanoScience. 2025(1). https://doi.org/10.1007/s12668-024-01703-7.
9. Akpeji BH, Bawa HA, Gbajabiamila AT, Elemike EE, Ogunsipe A, Amitaye AN, et al. Nanocomposites of tin hydroxide phthalocyanine Sn(OH) Pc and titanium dioxide nanoparticles for improved antimicrobial activities. J Inorg Organomet Polym Mater. 2025;35(2):1292–308. https://doi.org/10.1007/s10904-024-03291-1.
10. Kumar Chandraker S, Lal M, Kumar Ghosh M, Ram T, Paliwal R, Shukla R. Biofabrication of spherical silver nanoparticles using leaf extract of *Plectranthus barbatus* Andrews: characterization, free radical scavenging, and optical properties. Inorg Chem Commun. 2022;142:109669. https://doi.org/10.1016/j.inoche.2022.109669.
11. Manoharan S, Balakrishnan P, Sellappan LK. Fabrication of highly flexible biopolymeric chitosan/agarose based bioscaffold with Matricaria recutita herbal extract for antimicrobial wound dressing applications. Int J Biol Macromol. 2024;281:136195. https://doi.org/10.1016/j.ijbiomac.2024.136195.
12. Chandraker SK, Banu T, Tamang AM. Chapter 12 - Nanomaterial based on microorganisms for precision farming. In: Adetunji CO, Singh J, Singh KRB, Singh RP, Pandey SS, editors. Advances in Microbial Nanotechnology. Elsevier; 2026. p. 329–52. https://doi.org/10.1016/B978-0-443-31526-8.00015-7.
13. Phogat N, Kohl M, Uddin I, Jahan A. Chapter 11 - Interaction of Nanoparticles With Biomolecules, Protein, Enzymes, and Its Applications. In: Deigner H-P, Kohl M, editors. Precision Medicine. Academic Press; 2018. p. 253–76. https://doi.org/10.1016/B978-0-12-805364-5.00011-1.
14. Ikhuoria EU, Uwidia IE, Otabor GO, Ifijen IH. Comparative analysis of magnesium oxide nanoparticles biosynthesized from rubber seed shell and rubber leaf extracts. Biomed Mater Devices. 2024;2(2):1078–88. https://doi.org/10.1007/s44174-023-00139-z.
15. Joshi NC, Semwal P, Mitra D, Gururani P. A mini review on the synthesis, antimicrobial, and anticancer activities of Pd NPs. Discov Chem. 2025. https://doi.org/10.1007/s44371-025-00101-6.
16. Nguyen NYT, Grelling N, Wetteland CL, Rosario R, Liu H. Antimicrobial activities and mechanisms of magnesium oxide nanoparticles (nMgO) against pathogenic bacteria, yeasts, and biofilms. Sci Rep. 2018. https://doi.org/10.1038/s41598-018-34567-5.
17. Yılmaz GE, Göktürk I, Ovezova M, Yılmaz F, Kılıç S, Denizli A. Antimicrobial nanomaterials: a review. Hygiene. 2023. https://doi.org/10.3390/hygiene3030020.
18. Rani N, Singh P, Kumar S, Kumar P, Bhankar V, Kumar K. Plant-mediated synthesis of nanoparticles and their applications: A review. Mater Res Bull. 2023;163:112233. https://doi.org/10.1016/j.materresbull.2023.112233.
19. Kau N, Kumar R, Alhan S, Sharma H, Singh N, Yogi R, et al. *Lycium shawii* mediated green synthesis of silver nanoparticles, characterization and assessments of their phytochemical, antioxidant, antimicrobial properties. Inorg Chem Commun. 2024;159:111735. https://doi.org/10.1016/j.inoche.2023.111735.
20. Silva AA, Sousa AMF, Furtado CRG, Carvalho NMF. Green magnesium oxide prepared by plant extracts: synthesis, properties and applications. Mater Today Sustain. 2022;20:100203. https://doi.org/10.1016/j.mtsust.2022.100203.
21. Kaur N, Aditya RN, Singh A, Kuo TR. Biomedical applications for gold nanoclusters: recent developments and future perspectives. Nanoscale Res Lett. 2018;13(1):302. https://doi.org/10.1186/s11671-018-2725-9.
22. Chandraker SK, Lal M, Ghosh MK, Tiwari V, Ghorai TK, Shukla R. Green synthesis of copper nanoparticles using leaf extract of *Ageratum houstonianum* Mill. and study of their photocatalytic and antibacterial activities. Nano Express. 2020. https://doi.org/10.1088/2632-959X/ab8e99.
23. Hirphaye BY, Bonka NB, Tura AM, Fanta GM. Biosynthesis of magnesium oxide nanoparticles using *Hagenia abyssinica* female flower aqueous extract for characterization and antibacterial activity. Appl Water Sci. 2023. https://doi.org/10.1007/s13201-023-01987-2.
24. Chandraker SK, Kumar R. Biogenic biocompatible silver nanoparticles: a promising antibacterial agent. Biotechnol Genet Eng Rev. 2024;40(4):3113–47. https://doi.org/10.1080/02648725.2022.2106084.
25. Ananda A, Thippeswamy R, Puthran AS, Reddy LS, Shilpa BM. Green synthesis of MgO nanoparticles using Phyllanthus emblica for Evans blue degradation and antibacterial activity, in Materials Today: Proceedings, Elsevier Ltd, 2021, pp. 801–810. https://doi.org/10.1016/j.matpr.2021.05.340.
26. Gupta CL, Akhtar S, Kumar N, Ali J, Pathak N, Bajpai P. In silico elucidation and inhibition studies of selected phytoligands against mitogen-activated protein kinases of protozoan parasites. Interdiscip Sci Comput Life Sci. 2016;8(1):41–52. https://doi.org/10.1007/s12539-015-0269-6.
27. Kirubakaran D, Krishnan V. Toxicological profile and therapeutic potentials of Impatiens chinensis leaf extract: exploring antibacterial, antioxidant, antidiabetic and insecticidal properties. Pharmacol Res. 2025;7:100238. https://doi.org/10.1016/j.prenap.2025.100238.
28. Shah PTA, Khan MA, Zahid MU, Hussain SJ, Ali Z, Almaary KS, et al. Effect of surface capping on the antimicrobial, antiparasitic, and antioxidant properties of biocompatible magnesium oxide nanoparticles (MgO-NPs). 3 Biotech. 2025. https://doi.org/10.1007/s13205-025-04590-1.
29. Girma WM, Aragie MS, Berehe BA, Assen AH. Biogenic synthesis and characterization of MgO nanoparticles using *Verbascum sinaiticum*: antibacterial, free radical, and reactive oxygen species scavenging activities. Mater Adv. 2025;6(12):4003–15. https://doi.org/10.1039/d4ma01279h.
30. Patil PV, Nerleka N, Kuldeep A, Patil PP, Dandge PB, Dongale TD, Dandge P, Rashinka GS. *Terminalia bellirica* (Gaertn.) Roxb. extract-mediated green synthesis of magnesium oxide nanoparticles for multifunctional applications. Plant Nano Biol. 2024. https://doi.org/10.1016/j.plana.2024.100069.
31. Zhang Z, Liu D, Jiang J, Song X, Zou X, Chu S, et al. Metabolism of IMM-H004 and its pharmacokinetic-pharmacodynamic analysis in cerebral ischemia/ reperfusion injured rats. Front Pharmacol. 2019. https://doi.org/10.3389/fphar.2019.00631.
32. Waghmode MS, Gunjal AB, Mulla JA, Patil NN, Nawani NN. Studies on the titanium dioxide nanoparticles: biosynthesis, applications and remediation. SN Appl Sci. 2019. https://doi.org/10.1007/s42452-019-0337-3.
33. Danaei M, Dehghankhold M, Ataei S, Hasanzadeh DF, Javanmard R, Dokhani A, Khorasani S, Mozafari MR. Impact of particle size and polydispersity index on the clinical applications of lipidic nanocarrier systems. MDPI AG. 2018. https://doi.org/10.3390/pharmaceutics10020057.

34. Aravind M, Amalanathan M, Mary MSM. Synthesis of TiO2 nanoparticles by chemical and green synthesis methods and their multifaceted properties. SN Appl Sci. 2021. https://doi.org/10.1007/s42452-021-04281-5.
35. Ali S, Sudha KG, Thirumalaivasan N, Ahamed M, Pandiarai S, Rajeswari VD, et al. Green synthesis of magnesium oxide nanoparticles by using *Abrus precatorius* bark extract and their photocatalytic, antioxidant, antibacterial, and cytotoxicity activities. Bioengineering. 2023. https://doi.org/10.3390/bioengineering10030302.
36. Afuye and Olasunkanmi. Green synthesis of MgO Nanoparticles Using Anona Muricata Leaf Aqueous Extract and its Antidiabetic Activity, 2022. [Online]. Available: https://fpiwitedjournal
37. Jimoh AA, Akpeji BH, Azeez SO, Ayipo YO, Abdulsalam ZA, Adebayo ZF, et al. Biosynthesis of Ag and TiO2 nanoparticles and the evaluation of their antibacterial activities. Inorg Chem Commun. 2022. https://doi.org/10.1016/j.inoche.2022.109503.
38. Ogwuche CE, Elemike EE, Oju D, Onwudiwe DC, Singh N, Akpeji BH. Synthesis, characterization, anticancer and antimicrobial potentials of *Chrysothemis Pulchella* leaf extract mediated gold nanoparticles. J Inorg Organomet Polym. 2024;34:944–51. https://doi.org/10.1007/s10904-023-02817-3.
39. Akpeji BH, Emegha MC, Onyenue EE, Meshack OQ, Elemike EE. Synthesis and characterization of nanoparticles of ZnO, carbon dot and ZnO-Carbon dot nanocomposite from groundnut shell waste. J Appl Sci Environ Manage. 2024;28(6):1771–80. https://doi.org/10.4314/jasem.v28i6.16.
40. Akpeji BH, Jimoh AA, Akusu PO, Okhuarobo LO, Ayomanor BO, Okologume JO, Udoji NJ, Elemike EE. Microbial mediated fabrication of Ag and TiO_2 nanoparticles for bacterial inhibition. Int Res J Pure Appl Chem. 2025;26(2):56–72. https://doi.org/10.9734/irjpac/2025/v26i2905.
41. Gbajabiamila AT, Elemike EE, Akpeji BH, Bawa HA, Hossain I, Pere C, Anekwe-Nwekeaku OJ. Enhanced solar-assisted degradation of Sunset Yellow dye using plant-mediated Ag-TiO2/Na-BNT nanocomposite: synthesis, characterization, and performance optimization. J Hazard Mater Adv. 2025. https://doi.org/10.1016/j.hazadv.2025.100682.
42. Jimoh AA, Akpeji BH, Aduwa SI, Ogundele DT, Johnson MJ, Azeez SO, et al. Microbial assisted biogenic synthesis of titanium dioxide nanoparticles for enhanced methylene blue removal from aqueous solutions. Discov Chem. 2026;3:92. https://doi.org/10.1007/s44371-026-00541-8.
43. Ogeleka DF, Adedokun TG, Bawa HA. Akpeji synthesis and characterization of saw dust carbon-dots-titanium dioxide nanocomposites for cultivation of fluted pumpkin seedlings in crude oil contaminated soil". J Appl Sci Environ Manage. 2025;29(11):3465–70.
44. Tesi GO, Ukachuku S, Kpomah B, Overah LC, Akpeji BH, Dolor AO, et al. Synthesis and characterization of magnetite-*Eichornia Crassipes* nanocomposite by chemical co-precipitation method for various applications. J Chem Soc Nigeria. 2025;50(2):352–62.
45. Okorhi FB, Akpeji BH. Carbon dot soil enhancement: creating a new era of environmentally conscious and climate-adaptive agriculture. Global Res Environ Sustain. 2025;3(1):pp17-30.
46. Akpeji BH, Korede TB, Adedokun J. Removal of Mn (II) ions from aqueous solution using silver and titanium dioxide nanoparticles derived from bacterial pigment: experimental characterization and optimization. Adv Ind Eng Manag (AIEM). 2024;13(2):154–65. https://doi.org/10.7508/alem.02.2024.154.165.

Publisher's note

Springer Nature remains neutral with regard to jurisdictional claims in published maps and institutional affiliations.